Excess pCO_2 in Surface Seawater of the Arabian Gulf

Izumi, Connor[1];
Al-Thani, Jassem[2];
Yigiterhan, Oguz[2];
Al-Ansari, Ebrahim Mohd A S [2];
Vethamony, Ponnumony [2];
Sorino, Caesar Flonasca [2];
Anderson, Daniel B. [1];
Murray, James W. [1*]

1. **School of Oceanography, University of Washington, Box 355351, Seattle WA 98195, USA**

2. **Environmental Science Center, Qatar University, P.O. Box: 2713, Al-Tarfa, Doha, Qatar**

***Corresponding Author**
James W. Murray
School of Oceanography,
University of Washington,
Box 355351,
Seattle WA 98195
jmurray@uw.edu

Running head: Excess pCO_2

Key Points

1. pCO_2 in surface seawater in the Arabian Gulf averages about 460 μatm and is supersaturated with respect to the atmosphere
2. Salinity normalized total alkalinity (NTA) and dissolved inorganic carbon (NDIC), and the tracer ΔAlk*, suggest that $CaCO_3$ formation is the origin of this excess CO_2.
3. $CaCO_3$ formation in coral reefs is unlikely due to bleaching events and abiological heterogeneous calcite precipitation in the water column may be occurring.

ABSTRACT:

Dissolved inorganic carbon (DIC) and total alkalinity (TA) were sampled in December, 2018 and May, 2019 in the Exclusive Economic Zone (EEZ) of Qatar in the Arabian Gulf. pCO_2 calculated in surface seawater averaged 459 ± 61 μatm and was supersaturated with respect to the atmosphere. The region was degassing CO_2 to the atmosphere and the flux was about 1.25 mmol C m^{-2} d^{-1}. The origin of this excess CO_2 must be due to $CaCO_3$ precipitation. The horizontal relationship between salinity-normalized total alkalinity (NTA) and dissolved inorganic carbon (NDIC) showed that $CaCO_3$ formation was more important, relative to net biological productivity, than in the open ocean. The tracer Alk* has values primarily determined by $CaCO_3$ formation and values of Alk* ranged from -50 to -310 μmol kg^{-1}, which is consistent with substantial $CaCO_3$ formation. ΔAlk* increased with increasing distance northward from Hormuz. The rate of calcification calculated from the air-sea flux of CO_2 (5.6 mmol C kg^{-1} y^{-1}) and from ΔAlk* (5.9 mmol C kg^{-1} y^{-1}) agreed well. However, $CaCO_3$ formation by net calcification in coral reefs is unlikely as they have limited distribution and have been severely damaged by past coral bleaching. There are high concentrations of excess particulate Ca in the water column that cannot be accounted for by input of $CaCO_3$-rich Qatari dust. Carbonate forming plankton are absent in the water column. We propose that abiological, heterogeneous calcite precipitation (HCP) may be occurring. The mechanism is unknown but nucleation by $CaCO_3$-rich Qatari dust may assist this process.

250 / 250 words

Data Availability

The data used for preparing this study has been submitted to BCO-DMO and is being processed,

Plain Language Summary (<200 words)

Ocean acidification is a consequence of increased emissions of CO_2 to the atmosphere and is a major threat to marine ecosystems. Coral reefs in the Arabian Gulf have historically been a significant component of this warm and salty region's marine biological storehouse. Though ocean acidification is a concern, little is known about the carbonate system chemistry in these waters. The most recent previous data was from 1977 and techniques have improved since that time. An international collaboration between Qatar University and the University of Washington provided an opportunity to correct this deficiency. Samples for dissolved inorganic carbon and total alkalinity were collected in December, 2018 and May 2019. Values of pCO_2 in surface seawater were greater than atmospheric values indicating that the Gulf was not taking up atmospheric CO_2. Horizontal changes in DIC and TA indicate that $CaCO_3$ formation is occurring. The origin of the elevated pCO_2 must be due to $CaCO_3$ formation. However, carbonate forming plankton are not present and coral reefs, though abundant in the past, have been severely damaged by several bleaching events. One possible explanation is that abiological $CaCO_3$ formation is occurring in the water column, perhaps assisted by nucleation on $CaCO_3$-rich dust of land-based origin.

200/200 words

Index Terms

4825 Geochemistry
1050 Marine geochemistry (4835, 4845, 4850)
4220 Coral reef systems (4916)
4243 Marginal and semi-enclosed seas
0428 Carbon cycling (4806)

Keywords

pCO_2, Coral Reefs, Ocean Acidification, Calcification, Arabian Gulf

1. Introduction

There is concern that coral reefs in the Arabian (Persian) Gulf (hereafter referred to as 'Gulf') are being severely impacted by ocean acidification (Orr et al., 2005; Doney et al., 2009) yet little is known about the carbonate system geochemistry in this region. Reefs cover a relatively small area but they represent the region's biological storehouse. Many of the Gulf's fisheries depend on these habitats. It comes as a surprise to many that the Gulf is a repository of significant biodiversity. Historically, the countries bordering the Gulf exploited pearl oyster beds and coral reefs as a large part of their economy and cultural heritage. The World-Wide Fund for Nature (WWF) has identified the Gulf as part of a Global 200 Ecoregion - one of 43 priority marine ecosystems worldwide. Unfortunately, the coral reefs in this region have been severely impacted by degradation due to climate change and anthropogenic modifications.

The Gulf is a semi-enclosed marginal sea with an area of 240,000 km^2 and mean depth of 35m (Kampf and Sadrinasab, 2006; Vaughan et al., 2019). Most deeper areas of the Gulf are located along the Iranian coast whereas broad, shallow regions with depths less than 35 m are found along the coast of Arabian Peninsula. It has free exchange with the Gulf of Oman in the Arabian Sea through the Strait of Hormuz, which is 56 km wide and has a maximum depth of 100m (Al Ansari et al., 2015). The circulation in the Gulf is characterized as reverse estuarine. Lower salinity (S = 36.5) seawater enters at the surface through the Strait of Hormuz. The climate of this regions is very hot and dry and evaporation is estimated to be ~200 cm yr^{-1} for the central region of the Gulf (Al Ansari et al., 2015). Hence, the salinity and density increase due to evaporation as seawater flows to the north from the Strait. Higher salinity seawater ($S \geq 40$) exits at depth through the Strait. Due to geostrophy, the inflow of Indian Ocean Surface Water (IOSW) follows the Iranian coastline, whereas the denser bottom outflow follows the coastline of

134 the United Arab Emirates. The total volume of the Gulf is ~8,600 km^3 and the volume of the
135 deep outflow through Hormuz is about 6,620 km^3 y^{-1}. Therefore, the total residence time of the
136 Gulf's seawater is about 1.3 years (Sheppard et al., 2010). Residence time is a crucial factor
137 when considering the status of ocean acidification. Concentrations of carbonate system species in
138 the surface waters reflect a balance between the inputs through the Straits, enrichment due to
139 evaporation and the sources and sinks due to air-sea exchange and biological processes.
140 The carbonate system chemistry in the Gulf was first sampled in 1977 (Brewer and
141 Dyrssen, 1985) but has not been studied since. Surface water enters the Gulf with relatively high
142 concentrations of dissolved inorganic carbon (DIC) and total alkalinity (TA) from the Arabian
143 Sea. As the water flows northward, DIC and TA increase but salinity normalized DIC (NDIC)
144 and alkalinity (NTA) decrease. The decrease in concentrations of NDIC and NTA can be used to
145 determine the relative importance of CO_2 removal by $CaCO_3$ formation versus primary
146 production. Another factor to consider is that, as the water flows northward, some CO_2 is lost to
147 the atmosphere due to gas exchange. At the time of the Brewer and Dyrssen study in 1977, the
148 Arabian Gulf was degassing CO_2 to the atmosphere. Now, 40 years have passed and the
149 gradients and fluxes may have changed. Because data regarding the progress of ocean
150 acidification in the Arabian Gulf are sparse, an international collaboration between Qatar
151 University (QU) and the University of Washington (UW) provided an opportunity to alleviate
152 this deficiency.
153 The goal of this study was to assess the status of the ocean carbonate system in the
154 Exclusive Economic Zone of Qatar in the Arabian Gulf with respect to present and future
155 impacts by ocean acidification and use the horizontal distributions of DIC and TA to determine

156 the relative importance of organic matter production and $CaCO_3$ formation as sinks and sources
157 of CO_2.

158 **2. Methods**

159 **2.1 Samples**

160 Water column sampling was conducted, using 12, rosette mounted, 10-L PVC Niskin
161 bottles, on December 5, 2018 and May 18, 2019 in the Arabian Gulf on the RV Janan (Figure 1).
162 Surface seawater samples and hydrographic data were collected at seven stations (stations 1C,
163 2C, 3C, 4C, 5C, 6B, 6C) along a transect from the central east coast of Qatar across the Qatari
164 Exclusive Economic Zone (EEZ). Stations were chosen to be nearly perpendicular to the major
165 axis of the Gulf to capture main regional hydrographic features across the EEZ. The transect
166 provides a reasonable representation of hydrographic distributions across the wider part of the
167 Gulf. Samples were collected in triplicate at each station. Vertical profiles with one surface
168 sample, one bottom sample, and 1 to 3 mid-depth samples were collected at stations 2C, 4C, 6B,
169 and 6C.

170 Samples for DIC and TA were collected in 300 mL Wheaton BOD glass bottles with
171 ground glass stoppers. Samples were sealed immediately after collection to prevent loss of CO_2.
172 Samples were poisoned with 150 µL $HgCl_2$ (0.05% by volume) to prevent biological activity,
173 then covered with aluminum foil.

174

175

176 **2.2 Analyses**

177 The best approach for understanding ocean acidification is to measure the primary
178 capacity factors of the carbonate system chemistry which are dissolved inorganic carbon (DIC)

179 and total alkalinity (TA) (Stumm and Morgan, 1995). Being capacity factors means that they
180 behave conservatively during mixing, in the absence of gas exchange and biological processes.
181 DIC and TA may not be the most precise pair of variables for calculating pH, pCO_2 and
182 carbonate ion (Orr et al, 2018) but they were the most convenient parameters for us to measure
183 on samples collected in the Arabian Gulf and shipped to Seattle for analyses.
184 After collection, samples were shipped to the University of Washington for DIC and TA
185 analyses in Dr. Alex Gagnon's laboratory. Carbonate system measurements followed the
186 methods of Dickson et al. (2007). Briefly, TA (μmol kg^{-1}) was determined through open-cell
187 automated titration (876 Dosimat plus, Metrohm AG) with a 0.1M hydrochloric acid
188 (HCl)+0.6M sodium chloride (NaCl) solution. Total DIC (μmol kg^{-1}) was obtained through
189 coulometric determination (VINDTA 3D, Marianda with UIC coulometer). Certified reference
190 materials for TA and DIC obtained from Andrew Dickson (Scripps Institution of Oceanography)
191 were run in conjunction with seawater samples as a calibration standard and to monitor
192 precision. Long-term precision for DIC and TA in this lab, based on repeated measurements of
193 CRM materials, was ± 3.7 μmol kg^{-1} (2σ std. dev.) and ± 4.3 μmol kg^{-1} (2σ std. dev.),
194 respectively (Bolden et al., 2019).
195 pCO_2, pH and CO_3^{2-} were calculated from DIC and TA using CO2Calc on the total pH
196 scale with carbonate equilibrium constants refit from Mehrbach et al. (1973) by Dickson and
197 Millero (1987); borate alkalinity was calculated using the boron / chlorinity (salinity)
198 relationship provided by Lee et al. (2010) and equilibrium constants from Dickson (1990).
199 Where necessary, TA, and DIC values used in subsequent calculations were salinity-normalized
200 (NTA, NDIC) to a mean salinity value of 40.0. As there are no significant freshwater
201 contributions from rivers or groundwater in this region, the normalization relationship of Friis et

al (2003) was not necessary. During both cruises, hydrographic properties (temperature, practical salinity (S_p), O_2, pH, % transmission and fluorescence) were measured using a SeaBird Electronics, SBE 911 mounted on a SeaBird rosette. The pH sensor used in our project was a SBE 27 pH / O.R.P (Redox) Sensor. Dissolved oxygen was measured using the SBE 43 Dissolved Oxygen sensor. Discrete water samples were taken directly from the Niskin bottles and analyzed for dissolved oxygen within a few hours of collection using the Winkler titrimetric method (Carpenter, 1965). Nutrients (NO_3, NO_2, NH_4, soluble reactive phosphate (SRP) and Si) and chlorophyll were analyzed on filtered samples using classical techniques (Parsons et al., 1984).

Suspended particulate matter for particulate Ca analyses was sampled in 2012, at the same stations, on a previous cruise. Seawater was filtered directly from Niskin bottles through 47 mm filter holders and 0.45 μM mesh size Nuclepore filters (Yigiterhan et al., 2020). Filtration volumes of 2 L, provided sufficient samples for analyses. Particulate samples were acid digested in a clean lab on hot plates using trace metal grade concentrated HF (16.5M), HCl (6M) and, HNO_3 (16M) acids (Yigiterhan and Murray, 2008; Yigiterhan et al., 2011). H_2O_2 was added for complete removal of the organic material. Calcium analyses were done using ICP-OES with precision and accuracies of about 5%. Excess Ca concentrations (non-lithogenic) were calculated, as in Yigiterhan et al. (2020), by subtracting the lithogenic fraction using aluminum as a tracer and assuming that the composition of the lithogenic fraction can be represented by composition of average dust from Qatar (Yigiterhan et al., 2018).

$$Ca_{excess} = Ca_{total} - Al_{total} \times Ca/Al_{dust} \quad (1)$$

3. Results

The hydrographic (Station, Depth, T, S_p, O_2), nutrient (NO_3, SRP, H_4SiO_4) and carbonate system (DIC, TA) data are given in Table 1. Calculated pCO_{2calc} and pH_{calc} are also given in Table 1. The means and standard deviations are given for each cruise. As there was no statistical difference between the data from the two cruises, the data sets were combined for the interpretations.

Temperature ranged from 24.458° to 26.845°C and salinity (S_p) ranged from 40.290 to 40.994. DIC content ranged from 2065 to 2235 μmol kg^{-1}, and TA levels ranged from 2415 to 2601 μmol kg^{-1}. There was no systematic variation observed with depth. The nutrient concentrations were very low reflecting the oligotrophic nature of this water column. The regression of NO_3 versus SRP is not significant with R^2 = 24% (not shown). But, comparison of the measured data with the Redfield relationship (NO_3/SRP = 15) showed that the water column was nitrate deficient. This condition often favors nitrogen fixation (e.g., Deutsch et al., 2007), which has not been previously studied in the Gulf. Oxygen concentrations ranged from 176 to 202 μmol kg^{-1}, NO_3^- varied from 0.57 to 2.40 μmol kg^{-1}, NO_2^- from 0.09 to 1.44 μmol kg^{-1}, SRP from 0.06 to 0.93 μmol kg^{-1}, and dissolved silicate from 0.40 to 3.65 μmol kg^{-1}. % transmission ranged from 70.621% to 95.530%. Fluorescence ranged from 0.209 to 1.423, and chlorophyll levels ranged from 0.81 to 2.07 μgm kg^{-1}.

pCO_2, pH and CO_3^{2-} were calculated from DIC and TA. The pH measured by the SeaBird pH sensor (NBS scale) varied, from 8.13 to 8.22, but the pH_{calc} calculated from DIC and TA (total H scale) ranged between 7.93 and 8.12. Though accessible, pH sensors (SeaFET) can be inaccurate if sensor handling and calibration is not done with care (Miller et al., 2018). Because of these uncertainties, we used the values of pH_{calc} in this study. Calculated pCO_2 ranged from

390 to 582 μatm. The water column was supersaturated with respect to calcite ($\Omega_{calcite}$ = 4.97 to 6.95) and aragonite ($\Omega_{aragonite}$ = 3.32 to 4.62).

4. Discussion

4.1 pCO_2 in Surface Seawater

The partial pressures of carbon dioxide (pCO_2) in surface water of the Qatari EEZ in the central Arabian Gulf were higher than atmospheric pCO_2 during these study periods. The average surface concentrations were 478±80 μatm in November 2018 and 442±30 μatm in May 2019. Hence, the Gulf is a source of CO_2 to the atmosphere. Ocean acidification by local oceanic uptake of atmospheric CO_2 is not presently occurring. If atmospheric CO_2 continues to increase at its present rate the air-sea gradient will reverse and oceanic uptake of CO_2 will occur in approximately 2042. The question is "why are these surface waters supersaturated with CO_2?"

It is possible that the surface seawater entering through the Strait of Hormuz from the Gulf of Oman has been impacted by ocean acidification, resulting in higher DIC than pre-acidification. Thus, we can't absolutely rule out any impact from ocean acidification. Unfortunately, the source seawaters vary seasonally and their T, S and carbonate system compositions, appropriate for our study, are not available.

4.2 Alkalinity and DIC

The concentration of pCO_2 in seawater is controlled by the relative concentrations of carbonate Alk versus DIC. The relationship between TA and DIC in the Qatari EEZ is shown in Figure 2. There is essentially no statistical difference between the average values of TA and DIC for the two different sampling periods but we identify them separately in the figure. They were combined for the data analysis. Also shown are concentrations in the inflowing surface water at the Strait of Hormuz, which we assumed were the same as in Brewer and Dyrssen (1985). Both

TA and DIC increase after entering the Arabian Gulf, due to the increase in salinity due to evaporation.

To interpret the geochemistry of the carbonate system we normalizing individual concentrations to a constant salinity (S = 40). The resulting normalized values of NTA and NDIC are plotted in Figure 3. We also show the surface water concentrations from the Strait of Hormuz and the surface data, from 1977, in the Gulf from Brewer and Dyrssen (1985). The concentrations of NTA and NDIC decrease as surface seawater flows to the north after entering through Hormuz from the Arabian Sea. The combined data sets decrease with a slope of $\Delta NTA/\Delta NDIC = -0.65$. If we assume simple model reactions for formation of organic matter (CH_2O) and $CaCO_3$, the change in $CaCO_3$ formation and organic matter production can be predicted.

$$CO_2 + H_2O = CH_2O + O_2 \qquad \Delta DIC = -1 \quad \Delta TA = 0 \qquad (2)$$

$$Ca^{2+} + CO_3^{2-} = CaCO_3 \qquad \Delta DIC = -1 \quad \Delta TA = -2 \qquad (3)$$

The observed changes in NTA and NDIC, as surface seawater moves from the Strait of Hormuz to the Qatari EEZ, are consistent with a ratio of carbon uptake by $CaCO_3$ formation to carbon uptake by net photosynthesis ($\Delta CaCO_3$ / $\Delta OrgC$) of slightly greater than 0.6 (a ratio of about 1:2). For comparison, the average ratio for open ocean surface seawater, using this same approach, is about 1:18 (Emerson and Hedges, 2012). Therefore, carbon removal by $CaCO_3$ formation, relative to net photosynthesis, in the Gulf is about 12 times larger than in the open ocean.

293 This estimate neglects loss of CO_2 to the atmosphere by gas exchange and uptake by net
294 biological production. The characteristic residence time for gas exchange of CO_2 is slow, on the
295 time scale of one year. The residence time for the whole Arabian Gulf is about 1.3 years. Thus,
296 while we assume that loss of CO_2 is minor, some of the decrease in ΔNDIC may be due to gas
297 exchange and our estimates of the $\Delta CaCO_3$ / ΔOrgC should be considered an upper limit.
298 pCO_2 also becomes elevated in hypersaline reverse estuaries (e.g., Yao et al., 2020), but
299 as pCO_2 is controlled by the ratio of DIC / TA, it reflects DIC and TA consumption processes,
300 not the increase in S alone. Though S increases from S = 36.5 in the Gulf of Oman to S = 40.5 in
301 the Qatari EEZ this would not be considered a hypersaline environment.
302 The data from 1977 and 2018/2019 agree well. There has been no systematic change in
303 most of the NTA or NDIC data. The exception is that NTA in the 1977 data were lower for
304 NDIC concentrations less than ~2140 μmol kg^{-1}. These data are from the shallower region in the
305 Arabian Gulf to the NW of Qatar which may be anomalous because of freshwater input from
306 rivers in Kuwait. The ratio of $\Delta CaCO_3$ to ΔOrgC in 1977 of 2.5 was larger than for our combined
307 data sets in 2020, suggesting greater $CaCO_3$ removal in 1977 (Brewer and Dyrssen, 1985). That
308 may be because the Brewer and Dyrssen (1985) data included samples from the northwestern
309 part of the Arabian Gulf or it may suggest that $CaCO_3$ removal has decreased over the past
310 43years.
311 The slope of ΔNTA / ΔDIC (-0.65), and the corresponding $\Delta CaCO_3$ / ΔOrgC removal
312 ratios (1:2), can also be compared to those measured in healthy coral reef systems, elsewhere. In
313 the eastern central Red Sea, at Al-Fahal reef, the regression between NTA and NDIC was -0.42
314 (Saderne et al., 2019). This slope closely corresponds to the mean of the global coral reefs of
315 -0.41± 0.18 (Cyronak et al., 2018). A slope of 0.4 corresponds to $\Delta CaCO_3$ / ΔOrgC = 0.25. In

316 other words, one $CaCO_3$ removed per four organic carbon. At other locations, not strictly
317 comparable with the Arabian Gulf, a removal ratio of 2 was observed in the pristine Tetiaroa
318 Coral Atoll (Bolden et al., 2019) and a ratio of 2.3 was calculated for the coral reef system in
319 Kaneohe Bay, Hawaii (Fagan and Mackenzie., 2007). Though important, removal of C as $CaCO_3$
320 plays less of a role in the Gulf, than in healthy reef locations.

321 **4.3 Alk***

322 The tracer Alk* has values primarily determined by $CaCO_3$ precipitation and dissolution
323 (Carter et al., 2014). To define Alk***,** potential alkalinity (A_P) is calculated first to remove the
324 influence of nitrification (Brewer et al., 1975). Carter et al (2014) used an empirical relationship
325 that includes the combined effect of nitrate, sulfate and SRP (Kanamori and Ikegami, 1982).
326 Though derived for the North Pacific, this coefficient appears to be globally applicable (Wolf-
327 Gladrow et al., 2007). Potential alkalinity (A_P) is defined as:

328

329 $$A_P = TA + 1.26\,[NO_3] \quad (4)$$

330

331 where TA is total alkalinity and $[NO_3]$ is the concentration of nitrate (μmol kg^{-1}). To remove the
332 dependence on salinity, a background concentration, conservative potential alkalinity (A_P^C), is
333 calculated as:

334 $$A_P^C = S\,\frac{A'_P}{S'} = \text{S x } 66.40\ \mu\text{mol kg}^{-1} \quad (5)$$

335

336 where A'_P and S' are mean values for the whole surface ocean. Though our data is from a coastal
337 region, we assume this equation can be utilized as fresh water input is negligible. Carter et al
338 (2014) defined Alk* as the deviation of potential alkalinity from A_P^C.

$$Alk^* = A_P - A_P^C \quad (6)$$

$$= A_P - S \times 66.40\ \mu mol\ kg^{-1} \quad (7)$$

Regions with large net carbonate precipitation result in negative Alk*. All values of Alk* calculated for our data set were negative and ranged from -50 to -310 μmol kg^{-1}. This is consistent with substantial $CaCO_3$ formation in the Gulf. The Alk* values calculated using the same equations, by Carter et al. (2014) for the Red Sea and the Trucial Coast region (the Pirate Coast) of Oman in the Arabian Gulf were -247 μmol kg^{-1} and -240 μmol kg^{-1}, respectively.

In order to examine the spatial variability of how much $CaCO_3$ was precipitating in the Arabian Gulf itself, we calculated ΔAlk*, the difference between the specific locations in the Qatari EEZ and the surface water entering through the Strait of Hormuz. ΔAlk* increased with increasing distance northward from Hormuz to values as large as -310 μmol kg^{-1} (Figure 4). The average decrease of Alk* was -130 μmol kg^{-1}, which corresponds to a calcification of -65 μmol kg^{-1}.

The slope of ΔNTA versus ΔNDIC (corresponding to $\Delta CaCO_3/\Delta OrgC = 1:2$) and the negative values of Alk* suggest that large amounts of $CaCO_3$ are precipitating. This reaction, forming one mol of $CaCO_3$ produces one mole of CO_2 (equation 8), can explain why the concentrations of pCO_2 in the surface water are supersaturated.

$$2\ HCO_3^- + Ca^{2+} = CaCO_3 \downarrow + CO_2 \uparrow + H_2O \quad (8)$$

362 The precipitation of $CaCO_3$ is promoted by the elevated of the waters with respect to calcite
363 ($\Omega_{calcite}$ = 4.97 to 6.95) and aragonite ($\Omega_{aragonite}$ = 3.32 to 4.62).
364
365 **4.4 Air-Sea Flux of CO_2**
366 We calculated the flux of CO_2 across the air - sea interface as an estimate of the rate of
367 calcification. The flux was calculated using the stagnant boundary layer model for gas exchange
368 (e.g., Liss and Slater, 1974).
369
370 $$Flux_{CO2} = k\ K_H\ (pCO_{2sw} - pCO_{2atm}) = K\ \Delta pCO_2 \quad (9)$$
371
372 where k is the piston velocity (a function of wind speed), K_H is the solubility of CO_2 in seawater
373 (a function of T and S_p) and ΔpCO_2 is the gradient of CO_2 across the air-sea interface. We
374 assumed the annual average wind speed at Doha, Qatar of 8 knots (~4 m s^{-1}) (from Qatar Civil
375 Aviation Authority, https://qweather.gov.qa/ClimateInfo.aspx) which corresponds to a piston
376 velocity of k = 5 cm h^{-1} or 1.25 m d^{-1} (Wanninkhof, 1992). The solubility (K_H) of CO_2 for T =
377 25°C and S_p = 40 is about 20 x 10^{-3} mol kg^{-1} atm^{-1}. We assumed the average pCO_2 in surface
378 seawater was 450 μatm and atmospheric pCO_2 was 400 μatm and therefore, ΔpCO_2 = 50 μatm.
379 The resulting flux of CO_2 was -1.25 mmol C m^{-2} d^{-1} or -0.46 mol C m^{-2} y^{-1}. This is an
380 approximate calculation because it assumes representative concentrations and an average wind
381 speed. However, wind speed is variable and the relationship between k and windspeed is not
382 linear. It is also only an approximation as we only have two time points in the annual cycle.
383 During calcification, seawater becomes more acid due to the removal of bicarbonate and
384 carbonate ions, and this change in pH increases the abundance of dissolved CO_2 (Stumm and

385 Morgan 1995). The partial pressure of CO_2 increases and, in an open system, the CO_2 produced
386 is either taken up by biological production or escapes to the atmosphere. This simplistic
387 representation of the calcification process suggests that for each mole of $CaCO_3$ deposited, a
388 mole of CO_2 is liberated (Eqn. 8). The relationship is about 1:1 in freshwater but is reduced in
389 buffered seawater where only approximately 0.62 moles of CO_2 are liberated per mole of $CaCO_3$
390 deposited (Ware et al., 1991). Calculations show that the amount of CO_2 that must be released to
391 equilibrate seawater increases with increasing partial pressure of CO_2 in seawater (pCO_2)
392 (Frankignoulle et al., 1994). The calculation of the rate of calcification given here could be a
393 lower limit because we neglect CO_2 uptake by net biological production or could be an upper
394 limit as we neglect respiration of dissolved and particulate organic carbon.
395 If this calcification occurred in the water column with an average depth of 50m, the
396 volume rate would be 0.015 μmol kg^{-1} d^{-1} or 5.6 μmol C kg^{-1} y^{-1}. We can compare this with the
397 average decrease in Alk* of ΔAlk* = 130 μmol kg^{-1} (Section 4.3) which corresponds to a $CaCO_3$
398 formation rate of 65 μmol kg^{-1}. If we assume the seawater has a residence time of 1.3 years
399 (Sheppard et al., 2010), the $CaCO_3$ formation rate would be 5.0 μmol C kg^{-1} y^{-1}. Thus, the
400 $CaCO_3$ formation rate estimated from the CO_2 gas exchange flux and the decrease in ΔAlk*
401 agree well, in spite of many simplifying assumptions.
402 If this apparent net calcification rate was taking place in coral reefs uniformly spread over
403 the seafloor, the areal rates of CO_2 flux and calcification would be would be ~1.25 mmol m^{-2} d^{-1}
404 (0.46 mol C m^{-2} y^{-1}) and ~0.78 mmol m^{-2} d^{-1} (0.28 mol C m^{-2} y^{-1}), respectively. Studies of air-sea
405 CO_2 fluxes in seawater over healthy coral reef systems have given slightly larger, but
406 comparable results. There are lots of reasons why these comparisons are not valid, but they
407 provide a frame of reference for what fluxes might be possible if corals are producing the

$CaCO_3$. For example, the net annual area-specific flux of CO_2 to the atmosphere in Kaneohe Bay, Hawaii was 1.45 mol C m^{-2} y^{-1} (Fagan and Mackenzie, 2007) and 1.24 ± 0.33 mol m^{-2} y^{-1} using a much more extensive data set over a nine-year period (Terlouw et al., 2019). Lonborg et al (2019) calculated an average air-sea flux of CO_2 to the atmosphere in the Great Barrier Reef of 1.44 ± 0.15 mmol C m^{-2} d^{-1}. Though pCO_2 in seawater over growing corals varies on diurnal and seasonal time scales, on average it is greater than atmospheric pCO_2 and the fluxes given above are representative.

Calculation of the air-sea flux of CO_2 appears to suggest a reasonable rate of calcification but doesn't resolve the question about whether that calcification is occurring in the water column or sediments.

4.5 Corals in the Qatari EEZ

The magnitude of the apparent rate of net calcification at the sediment water interface calculated from the air-sea flux of CO_2 for the Qatari EEZ is plausible. We know that despite the extreme environmental conditions, the Gulf contains 40 species of *scleractinian* (hard) corals and 35 species of *alcyonacean* (soft) corals (Vaughan et al., 2019). Spatial patterns of corals broadly follow environmental conditions, with the highest diversity occurring near the Strait of Hormuz and along the Iranian coast where environmental conditions are more favorable. Most of the other healthy corals occur along the Trucial Coast of the United Arab Emirates (UAE) in the SW Arabian Gulf. These UAE coral reefs were once extensive but have declined dramatically in the past three decades due to bleaching events (Grizzle et al., 2016).

The coral reefs around Qatar were a valuable economic resource in the past. Historically, coral communities around Qatar were among the most widespread in the region. These coral

communities were dominated by *Acropora* (staghorn) table corals to water depths of 4-5m and massive *Porites* corals from 5m to 10m. They were described as "extensive" and "lush" (Rezal et al., 2004; Burt et al., 2015).

Unfortunately, there has been a general decline in the ecological health of corals in the Qatari region of the Gulf in recent decades. It is hypothesized that net calcification, growth rate and mortality of coral reefs have been adversely affected by bleaching events caused by extreme ocean warming. Severe damage occurred to corals as a result of recurrent bleaching events in 1996, 1998, 2002 and 2017 when sea surface temperature (SST) sometimes reached >37°C. These bleaching events resulted in near total loss of all coral from shallow (<3 m) habitats around Qatar. The damage due to bleaching was exacerbated by anthropogenic activities - sedimentation from dredging and pollution from the growing industrial sectors. The near-shore coral communities across much of eastern Qatar have become functionally extinct. Off-shore coral assemblages were also impacted by the bleaching events, but a few isolated, healthy sites exist, like Umm Al-Arshan (Burt et al., 2015) and Halul Island (Abdel-Moati, 2006). However, most off-shore sites (e.g., Fuwaurit and Al-Ashat) are covered by bare rock, sand, algal turfs and dead coral rubble (Burt et al., 2015; Sheppard et al., 2010).

The available data on the distribution and health of Qatari corals suggest that formation of $CaCO_3$ in coral reefs is an unlikely origin for the excess pCO_2 in the surface seawater.

4.6 Particulate Ca in the water column

A recent study of the composition of particulate matter in the Qatari EEZ showed that average Ca concentrations in the suspended particulate matter were high (3.6% by mass of particulate matter), and acid soluble (Yigiterhan et al, 2020). Though there is a significant amount of particulate Ca in the water column, its minerology has not been determined.

Biological studies reveal that carbonate forming plankton are absent (Quigg et al., 2013; Polikarpov et al., 2016). We considered that the particulate Ca comes from the abundant carbonate-rich atmospheric dust in this region (Yigiterhan et al., 2018). However, using Al as a tracer for dust, and the average Ca/Al ratio in Qatari dust, can only explain about 3% of the particulate Ca in water column particulate matter. So, there is excess $CaCO_3$ in the water column that does not appear to come from either plankton or Qatari dust.

4.7 Heterogeneous calcite precipitation (HCP)

It is possible that the excess CO_2 is due to abiological $CaCO_3$ formation in the water column. Such abiological $CaCO_3$ formation (also called heterogeneous calcite precipitation, HCP) was hypothesized by Wurgaft et al. (2016) to occur in the water column of the Red Sea. They interpreted water column data for NTA and NDIC in the Red Sea and the Gulf of Aqaba as indicating that heterogeneous $CaCO_3$ precipitation (HCP) was occurring. As HCP does not normally occur in supersaturated seawater due to inhibition by Mg^{2+} ions (Bischoff, 1977), even with $\Omega > 5$ (Berner, 1975), they argued that this HCP was induced by suspended sediments from flash floods or input of atmospheric dust. Comparisons of the Arabian Gulf and the Red Sea is difficult as the Red Sea is much deeper (>2000m). Nevertheless, the Arabian Gulf and Red Sea are similar in that both have reverse estuarine circulation driven by an increase in salinity due to evaporation in the northern end, growth of corals in shallow waters (Saderne et al., 2019) and large inputs of atmospheric dust. The apparent formation of $CaCO_3$ in the deep waters of the Red Sea (below the euphotic zone) was a key aspect of the argument for abiogenic HCP forming in that region.

The case has also been made that abiological, nonskeletal $CaCO_3$ formation occurs in the Grand Bahama Bank, east of the Florida Straits (Swart et al., 2014). In that region, the input of dust from North Africa was hypothesized to play an important role as both heterogeneous nucleation sites and as a source of iron, that would stimulate nitrogen fixation and biological production in this otherwise oligotrophic ocean region.

5. Conclusions

pCO_2 is supersaturated relative to atmospheric pCO_2 in the surface seawater of the Arabian Gulf. The relationship between NAlk and NDIC and values of ΔAlk* indicate that substantial $CaCO_3$ precipitation is occurring. The rate of $CaCO_3$ formation calculated from the air-sea flux of CO_2 and the decrease in the tracer ΔAlk* agree well. Removal by coral reefs looks unlikely, as healthy, growing corals are rare due to several recent bleaching events. There is excess, acid soluble, particulate calcium in the water column that cannot be explained as originating from carbonate forming plankton or $CaCO_3$-rich Qatari dust. The saturation states of waters with respect to calcite ($\Omega_{calcite}$ = 4.97 to 6.95) and aragonite ($\Omega_{aragonite}$ = 3.32 to 4.62) are high in the Gulf and perhaps the $CaCO_3$ rich dust can overcome the kinetic inhibition seen in the open ocean. $CaCO_3$ formation in the open ocean is typically biologically mediated. The evidence from this study suggests that heterogeneous calcite precipitation (HCP) could possibly be occurring in the Gulf, as hypothesized previously for the Red Sea. This HCP process may be aided by nucleating sites provided by dust input. If so, inorganic precipitation may play a more important role in coastal regions with significant dust input than previously thought.

References

Abdel-Moati, M. (2006). Coral Reef Conservation in Qatar, Marine Conservation Forum. EWS-WWF, Abu Dhabi, UAE, pp. 1–34.

Al-Ansari, E. M. A. S., Rowe, G., Abdel-Moati, M. A. R., Yigiterhan, O., Al-Maslamani, I., Al-Yafei, M. A., Al-Shaikh, I., Upstill-Goddard, R. (2015). Hypoxia in the central Arabian Gulf exclusive economic zone (EEZ) of Qatar during summer season, Estuar. Coast. Shelf S., 159, 60–68, https://doi.org/10.1016/j.ecss.2015.03.022, 2015.

Berner, R. (1975). The role of magnesium in the crystal growth of calcite and aragonite from sea water. Geochim. Cosmochim. Acta 39, 489–504.

Bolden I.W., Sachs, J.P. & Gagnon, A.C. (2019). Temporally-variable productivity quotients on a coral atoll: Implications for estimates of reef metabolism. Marine Chemistry 217, 1-13.

Brewer, P. G. & Dyrssen, D. (1985), Chemical oceanography of the Persian Gulf. Prog. Oceanogr., 14, 41–55

Burt, J. (2014). The environmental costs of coastal urbanization in the Arabian Gulf. City: Analysis of Urban Trends, Culture, Theory, Policy, Action 18 pp. 760–770.

521 Burt, J. A., Smith, E. G., Warren, C., & Dupont, J. (2016). An assessment of Qatar's coral
522 communities in a regional context. Marine Pollution Bulletin, 105, 473–479.
523
524 Carpenter, J. H. (1965). The Chesapeake Bay Institute technique for the Winkler dissolved
525 oxygen method. Limnol. and Oceanogr. 10, 141-143.
526
527 Carter, B.R., Toggweiler, J.R., Key, R.M., & Sarmiento, J.L. (2014). Processes determining the
528 marine alkalinity and calcium carbonate saturation state distributions. Biogeosciences, 11, 7349-
529 7362.
530
531 Cyronak, T., Andersson, A. J., Langdon, C., Albright, R., Bates, N. R., Caldeira, K., et al.
532 (2018). Taking the metabolic pulse of the world's coral reefs. PLoS ONE, 13(1), 1–17.
533 https://doi.org/10.1371/journal.pone.0190872
534
535 Deutsch, C., Sarmiento, J.L., Sigman, D.M., Gruber, N., & Dunne, J.P. (2007) Spatial coupling
536 of nitrogen inputs and losses in the ocean. Nature 445, 163–167
537
538 Dickson, A.G. (1990). Thermodynamics of the dissociation of boric acid in synthetic seawater
539 from 273.15 to 318.15 K. Deep Sea Res.. 37, 755–766. https://doi.org/10.1016/0198-
540 0149(90)90004-F.
541
542 Dickson, A.G., Sabine, C.L., & Christian, J.R. (2007). Guide to best practices for ocean CO2
543 measurements. PICES Special Publication 3.
544

545 Dickson, A.G. & Millero, F.J. (1987). A comparison of the equilibrium constants for the
546 dissociation of carbonic acid in seawater media. Deep Sea Res., 34, 1733–1743.
547 https://doi.org/10.1016/0198-0149(87)90021-5.
548
549 Doney, S.C., Fabry, V.J., Feely, R.A., & Kleypas, J.A. (2009). Ocean acidification: the other
550 CO_2 problem. Annu. Rev. Mar. Sci. 1, 169–192.
551
552 Emerson, S. & Hedges, J. (2012). Chemical Oceanography and the Marine Carbon Cycle.
553 Cambridge University Press. 453pp
554
555 Fagan, K. E. & Mackenzie, F. T. (2007). Air-sea CO2 exchange in a subtropical
556 estuarine-coral reef system, Kaneohe Bay, Oahu, Hawaii. Mar. Chem. 106, 174–191.
557 doi: 10.1016/j.marchem.2007.01.016
558
559 Frankignoulle, M., Canon, C. & Gattuso, J-P. (1994) Marine calcification as a source of carbon
560 dioxide: Positive feedback of increasing atmospheric CO_2. Limnology and Oceanography. 39,
561 458-462
562
563 Grizzle, R.L., Ward, K.M., AlShihi, R.M.S., & Burt, J.A. (2016). Current status of coral reefs in
564 the United Arab Emirates: Distribution, extent, and community structure with implications for
565 management. Marine Pollution Bulletin. 105, 515-523.
566

Kampf J. & Sadrinesab, M. (2006). The circulation of the Persian Gulf: a numerical study. Ocean Science, 2, 27-41

Kanamori, S. & Ikegami, H. (198. Calcium-alkalinity relationship in the North Pacific, J. Oceanogr., 38, 57–62, 1982.

Lee, K., Kima, T-W., Byrne R.H. , Millero, F.J. , Feely, R.A., & Liu, Y-M. (2010). The universal ratio of boron to chlorinity for the North Pacific and North Atlantic oceans. Geochimica et Cosmochimica Acta, 74, 1801-1811.

Liss P.S. & Slater P.G. (1974). Flux of Gases across the Air-Sea Interface. Nature 247, 181-184.

Lonborg C., Calleja, M.L.I., Fabricius, K,E., Smith, J.N., & Achterberg, E.P. (2019). The Great Barrier Reef: A source of CO_2 to the atmosphere. Marine Chemistry 210, 24-33.

Mehrbach, C., Culberson, C.H., Hawley, J.E., & Pytkowicx, R.M. (1973). Measurement of the apparent dissociation constants of carbonic acid in seawater at atmospheric pressure. Limnol. Oceanogr. 18, 897–907. https://doi.org/10.4319/lo.1973.18.6.0897.

Orr, J. C., Fabry, V. J., Aumont, O., Bopp, L., Doney, S. C., Feely, R. A., et al. (2005). Anthropogenic ocean acidification over the twenty-first century and its impact on calcifying organisms, Nature, 437, 681–686

589 Orr, J.C., Epitalon, J-M., Dickson, A.G., & Gattuso, J-P. (2018). Routine uncertainty propagation
590 for the marine carbon dioxide system. Marine Chemistry, 207, 84-107
591
592 Parsons T.R., Maita Y., & Lalli, G.M. (1984). A manual of chemical and biological methods for
593 seawater analysis. Pergamon Press, Oxford
594
595 Polikarpov,I., Saburova, M., & Al-Yamani, F. (2016). Diversity and distribution of winter
596 phytoplankton in the Arabian Gulf and the Sea of Oman. Continental Shelf Research, 119, 85-99.
597
598 Quigg, A.,Al-Ansi,M., NourAlDin,N., Wei,C.-L., Nunnally,C.C., Al-Ansari,I.S., Rowe, G.T. et
599 al. (2013). Phytoplankton along the coastal shelf of an oligotrophic hypersaline environment in a
600 semi-enclosed marginal sea: Qatar (Arabian Gulf). Cont. Shelf Res. 60, 1–16.
601
602 Rezai, H., Wilson, S., Claereboudt, M., & Riegl, B., (2004). Coral reef status in the ROPME sea
603 area: Arabian/Persian Gulf, Gulf of Oman and Arabian Sea. In:Wilkinson, C. (Ed.), Status
604 of Coral Reefs of the World: 2004. Australian Institute of Marine Science, Townsville,
605 pp. 155–169.
606
607 Saderne, V., Baldry, K., Anton, A., Agustí, S., & Duarte, C. M. (2019). Characterization of the
608 CO2 system in a coral reef, a seagrass meadow, and a mangrove forest in the central Red Sea.
609 Journal of Geophysical Research: Oceans, 124, 7513–7528.
610 https://doi.org/10.1029/2019JC015266
611

612 Sheppard, C., Al-Husiani, M., Al-Jamali, F., Al-Yamani, F., Baldwin, R., Bishop, J., et al.
613 (2010). The Gulf: a young sea in decline. Mar. Pollut. Bull. 60, 13–38.
614
615 Stumm, W. & Morgan, J.J. (1995) Aquatic Chemistry: Chemical Equilibria and Rates in Natural
616 Waters 3rd Edition. Wiley-Interscience pp, 1040
617
618 Swart, P.K., Oehlen, A.M., Mackenzie, G.J., Eberli, G.P., & Reijmer, J.J.G. (2014) The fertilization
619 of the Bahamas by Saharan Dust: A trigger for carbonate precipitation. Geology, 42: 671-674.
620
621 Terlouw G.J., Knor L.A.C.M., De Carlo E.H., Drupp P.S., Mackenzie F.T., Li Y.H., Sutton A.J.,
622 Plueddemann A.J., & Sabine C.L. (2019). Hawaii Coastal Seawater CO2 Network: A Statistical
623 Evaluation of a Decade of Observations on Tropical Coral Reefs. Front. Mar. Sci. 6, 226.
624 doi: 10.3389/fmars.2019.00226
625
626 Vaughan, G.O., Al-Mansoori, N. & Burt, J.A. (2019). The Arabian Gulf. World Seas: An
627 Environmental Evaluation. Pp, 1-23. https://doi.org/10.1016/B978-0-08-100853-9.00001-4
628 Elsevier.
629
630 Wanninkhof, R. (1992). Relationship between wind speed and gas exchange over the ocean. J.
631 Geophys. Res. 97, 7373–7382.

632 Ware, J. R., Smith S.V. & Reaka-Kudla, M.L. (1991) Coral reefs: sources or sinks of
633 atmospheric CO_2? Coral Reefs, 11, 127-130

Wolf-Gladrow, D.A., Zeebe, R.E., Klaas, C., Koertzinger, A., & Dickson, A.G., (2007). Total alkalinity: the explicit conservative expression and its application to biogeochemical processes. Mar. Chem. 106, 287–300.

Wurgaft E., Steiner, Z., Luz, B., & Lazar, B. (2016). Evidence for inorganic precipitation of $CaCO_3$ on suspended solids in the open water of the Red Sea. Marine Chemistry, 186, 145-155.

\Yao H., McCutcheon M.R., Staaryk C.J., & Hu X. (2020). Hydrologic controls on CO_2 chemistry and flux in subtropical lagoonal estuaries of the northwestern Gulf of Mexico. Limnol Oceanogr. 65: 1380-1398

Yigiterhan O., Alfoldy B.Z, Giamberini M., Turner J.C., Al-Ansari E.S., Abdel-Moati M.A., Al-Maslamani I.A., Kotb M.M., Elobaid E.A., Hassan H.A., Obbard J.P., & Murray J.W., (2018). Geochemical Composition of Aeolian Dust and Surface Deposits from the Qatar Peninsula. Chemical Geology 476, 24-45

Yigiterhan O. Al-Ansari, E.M.A.S., Nelson, A., Abdel-Moati, M.A.R., Turner, J., Alsaadi, H.A., Paul, B., Al-Maslamani, I.A., Al-Yafei, M.A.A.A., & Murray, J.W. (2020). Trace element composition of size-fractionated suspended particulate matter samples from the Qatari Exclusive Economic Zone of the Arabian Gulf: the role of atmospheric dust. Biogeosciences. 17, 381-401.

Acknowledgments

Alex Gagnon (UW) for providing the analytical facility for alkalinity and dissolved inorganic carbon analyses. We utilized the financial sources of IRCC International Research Co-Fund Collaboration Program of QU (Project No. IRCC-2019-002) for the cruise preparation, sampling and shipping. Discussions with Katie Shamberger (Texas A&M), Alex Gagnon (UW) and Isaiah Bolden (UW) improved the discussion.
.

Competing Interests

None of the authors have financial and personal competing interests to declare.

Author Contributions

J.W.M. and O.Y. designed the research. Samples were collected by J.A-T, O.Y., E.A-A, and C.S. Hydrographic data was processed by C.S. Nutrient analyses were conducted by J.A-T. J.W.M. wrote the manuscript. All authors edited the manuscript.

Table 1. Water column data from November 2018 and May 2019. The units for O_2, NO_3, soluble reactive phosphate (SRP), SiO_2, DIC and TA are all µmol kg^{-1} The units for pCO_2 are µatm. The grand averages for the combined data sets are DIC = 2180 ± 40µmol kg^{-1}. Alk = 2532 ± 30 µmol kg^{-1} and pCO_2 = 459 ± 61 µatm. Samples from the surface, middle and bottom of the water column are colored blue, orange and green, respectively

Data from November 2018											
Station	Depth	Temperature	Salinity	O2	NO3	PO4	SiO2	DIC	ALK	pCO2	pHcalc
1C	1.8	24.621	40.983	197	1.18	0.08	1.07	2065	2426	390	8.047
1C	10.3	24.458	40.994	196	1.61	0.33	1.38	2085	2415	438	8.004
2C	1.5	25.550	40.766	198	1.39	0.20	0.50	2128	2517	387	8.064
2C	22.3	24.900	40.855	191	1.09	0.06	0.64	2134	2514	391	8.059
3C	1.4	26.683	40.641	201	0.75	0.07	0.40	2197	2531	514	7.967
3C	15	26.314	40.625	195	1.27	0.37	0.50	2208	2528	537	7.951
3C	30	25.756	40.667	176	0.77	0.19	1.00	2150	2528	410	8.046
4C	1.8	26.819	40.565	202	0.57	0.16	1.44	2150	2530	426	8.033
4C	12.4	26.686	40.557	198	1.25	0.19	1.19	2154	2533	426	8.033
4C	36.9	26.669	40.557	190	1.28	0.20	1.85	2152			
5C	1.7	26.845	40.604	193	1.29	0.17	1.34	2213	2533	549	7.944
5C	15	26.822	40.602	191	1.77	0.31	0.90	2214	2530	561	7.936
5C	30.2	26.791	40.594	185	1.52	0.22	1.33	2148			
5C	51	26.796	40.595	184	1.68	0.22	0.98	2149	2535	416	8.041
6C	1.6	26.770	40.479	187	1.54	0.36	1.38	2230	2536	583	7.925
6C	18.3	26.773	40.478	188	1.89	0.26	0.84	2161	2540	431	8.031
6C	33.5	26.821	40.520	183	1.18	0.29	0.67	2224	2538	569	7.933
6C	53.3	26.843	40.531	181	2.40	0.23	1.40	2223	2538	564	7.936
6B	1.4	26.212	40.295	191	1.48	0.24	0.68	2164	2601	351	8.112
6B	20.4	26.219	40.291	187	1.66	0.21	0.72	2167	2542	429	8.037
6B	40	26.217	40.292	184	1.63	0.21	0.79	2233	2539	572	7.935
6B	57.5	26.218	40.290	182	2.03	0.28	3.65	2164	2543	422	8.042
6B	1.4	26.212	40.295	191	1.49	0.93	1.65	2232	2538	573	7.933
6B	57.5	26.218	40.290	182	1.86	0.22	2.56	2235	2540	575	7.933
Average								2174	2526	478	7.997
Std. Dev								47	38	80	0.058
Data from May 2019											
Station	Depth	Temperature	Salinity	O2	NO3	PO4	SiO2	DIC	ALK	pCO2	pHcalc
1C	1.7	27.043	41.026	190	0.54	0.35	2.64	2198	2556	483	7.988
1C	10	26.730	40.999	186	0.62	0.73	1.17	2197	2557	474	7.995
2C	1.6	27.599	40.757	207	4.22	1.44	2.21	2163	2552	434	8.027
2C	21.8	25.138	41.128	177	0.63	0.05	0.73	2206	2548	478	7.991
3C	1.7	27.527	40.451	211	0.86	0.05	0.63	2155	2546	424	8.038
3C	15.3	24.380	40.862	202	2.12	0.46	1.04	2214	2563	453	8.016
3C	29.6	24.505	41.201	166	0.94	0.36	1.05	2222	2555	485	7.987
4C	1.8	27.320	39.597	199	2.35	0.52	0.98	2134	2528	406	8.06
4C	15.8	23.387	40.310	229	1.65	0.29	1.24	2188	2548	409	8.056
4C	37	23.797	40.747	177	1.70	0.54	1.64	2215	2547	470	8.002
5C	1.6	27.124	39.274	161	1.76	2.29	1.60	2138	2513	429	8.042
5C	15.8	23.601	39.870	169	1.27	0.47	1.30	2171	2535	400	8.067
5C	32.6	22.600	40.190	138	1.61	0.57	2.63	2200	2535	434	8.035
5C	50.6	22.185	40.275	128	1.44	0.71	3.08	2203	2543	422	8.046
6C	1.8	27.263	39.304	131	2.25	0.14	0.77	2143	2505	450	8.024
6C	14.4	25.015	39.640	146	0.96	0.55	0.93	2169	2518	443	8.03
6C	33.3	21.252	40.075	143	3.54	0.80	2.81	2218	2538	441	8.032
6C	58.5	21.421	40.593	115	3.24	0.74	4.20	2214	2546	427	8.04
6B	1.7	27.297	39.361	185	1.51	0.22	0.63	2146	2509	452	8.023
6B	18.2	23.136	39.889	181	1.30	0.32	0.68	2152	2526	373	8.09
6B	34.4	21.400	40.032	137	2.17	1.13	1.90	2222	2535	456	8.021
6B	58.5	20.794	40.624	119	4.14	0.85	4.05	2227	2545	442	8.027
6B	1.7	27.297	39.361					2142	2474	500	7.983
6B	58.5	20.794	40.624					2227	2551	432	8.036
Average								2186	2536	442	8.027
Std. Dev								32	21	30	0.027

Figure 1: Station locations sampled in November 2018 and May 2019 in the Qatari Exclusive Economic Zone (EEZ) of Qatar in the Arabian Gulf

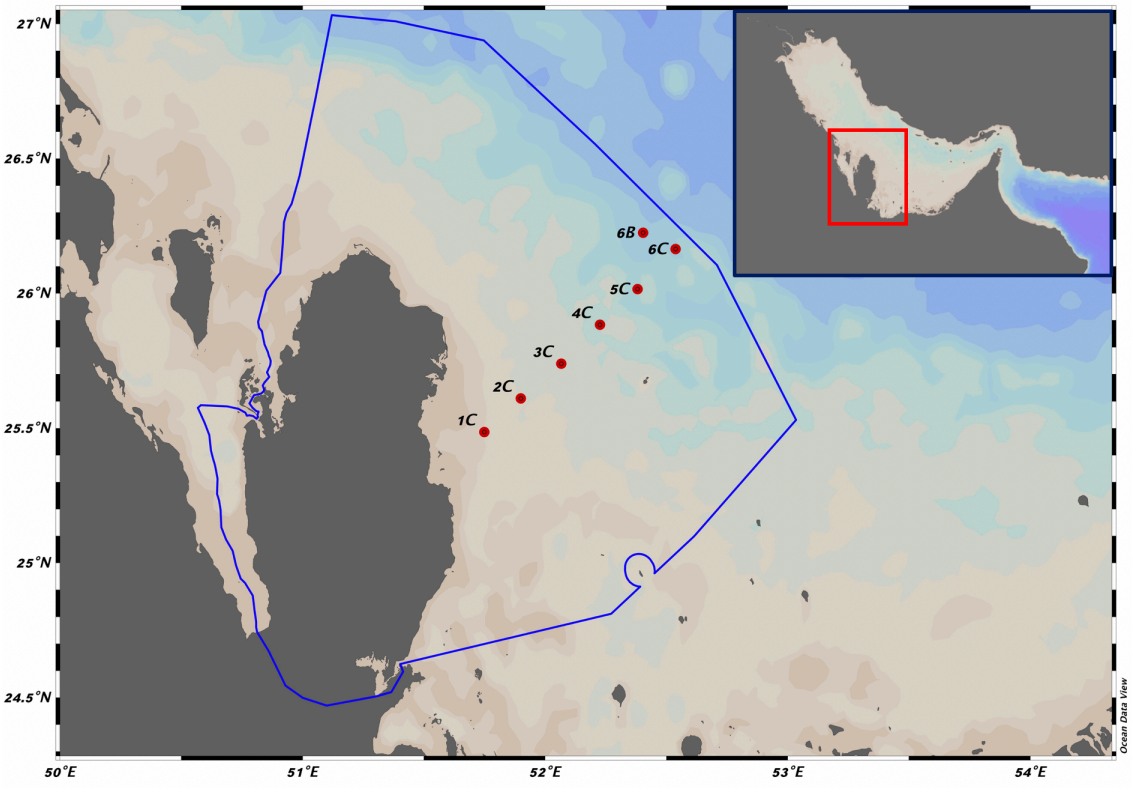

Figure 2. Alk versus DIC in the Exclusive Economic Zone (EEZ) of Qatar in the Arabian Gulf. The units for Alk and DIC are µmol kg^{-1}. The data point for 1977 from the Strait of Hormuz is from Brewer and Dyrssen (1985)

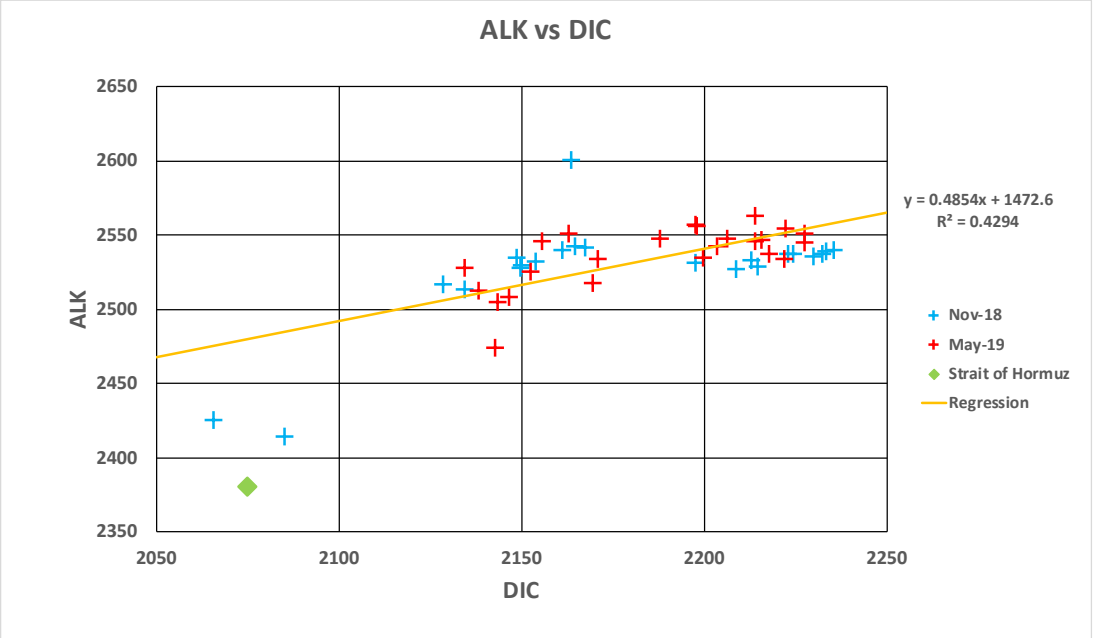

Figure 3. NAlk versus NDIC in the Qatari EEZ of the Arabian Gulf in November 2018 and May 2019. Data from 1977 for the entire Arabian Gulf and Strait of Hormuz by Brewer and Dyrssen (1985) are shown for comparison. The units for NAlk and NDIC are µmol kg^{-1}. The slope of the best fit regression (0.65) corresponds to a $\Delta CaCO_3$ / $\Delta OrgC$ removal ratio of ~1:2.

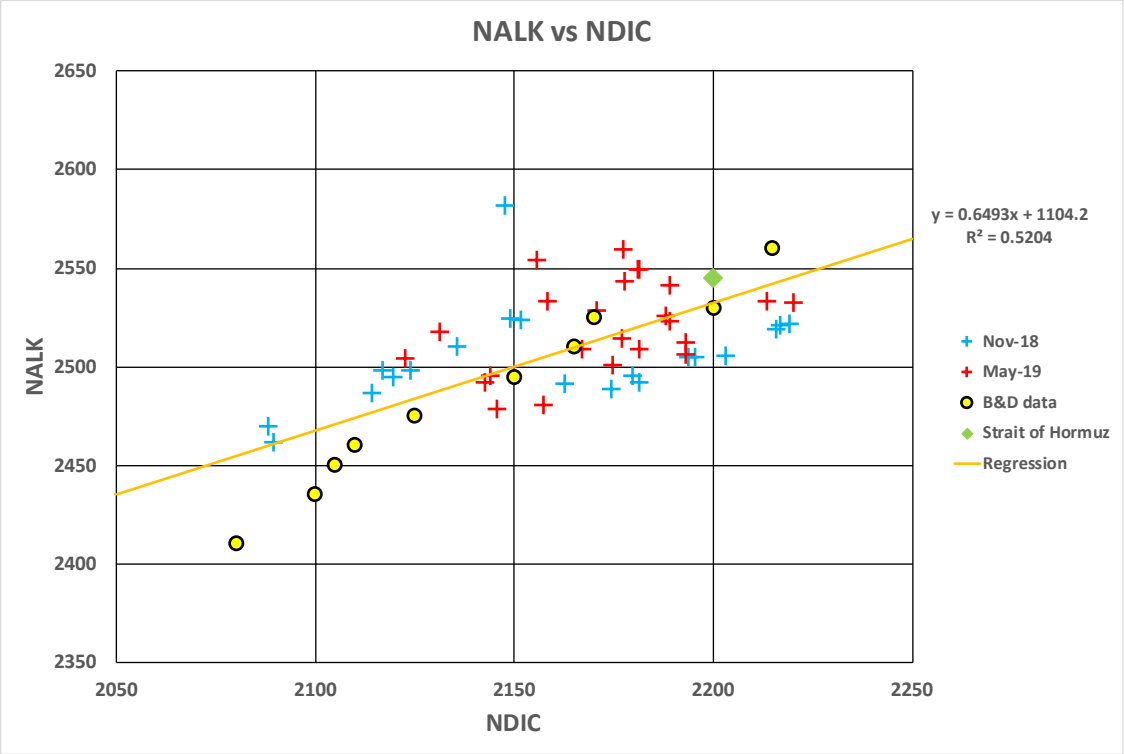

Figure 4. ΔAlk* in the Qatari EEZ, calculated as the difference between the value of Alk* at individual stations and the value for the Strait of Hormuz. ΔAlk* is plotted versus distance from the Strait of Hormuz. The gradual decrease in ΔAlk* indicates progressive precipitation of $CaCO_3$.